18TH WORLD CONFERENCE ON EARTHQUAKE ENGINEERING
WCEE2024
MILAN

MILAN, ITALY
30TH JUNE - 5TH JULY 2024

www.wcee2024.it

ASSESSMENT OF POST-LIQUEFACTION CONSOLIDATION SETTLEMENTS AFTER THE 2012 EMILIA EARTHQUAKE

M. Albano[1], A. Chiaradonna[2], M. Saroli[3,1], M. Moro[1], G. Solaro[4] & A. Pepe[4]

[1] Istituto Nazionale di Geofisica e Vulcanologia, Roma, Italy, matteo.albano@ingv.it

[2] Università degli Studi dell'Aquila, L'Aquila, Italy

[3] Università degli Studi di Cassino e del Lazio Meridionale, Cassino, Italy

[4] Istituto per il Rilevamento Elettromagnetico dell'Ambiente (IREA), Napoli, Italy

Abstract: *An earthquake with a magnitude of 5.8 struck the Emilia-Romagna region in northern Italy on 20 May 2012, resulting in significant damage and loss of life. In the days following the main shock, the rupture spread eastward and downward along the Ferrara thrust system, and westward along the neighbouring Mirandola thrust, leading to another earthquake of magnitude 5.6 on 29 May. After the initial earthquake, a number of postseismic events occurred. Wells in the vicinity of the epicentre experienced a sudden rise in water levels, followed by a gradual decline that did not return to preseismic levels within the observation period. Some wells even expelled a mixture of water and sand, and over 700 instances of liquefaction were observed. We conducted a study on the displacement of the Earth's surface during and after the Emilia 2012 seismic sequence, using a dataset comprising 18 synthetic aperture radar (SAR) images obtained from the descending orbit of COSMO-SkyMed (CSK) constellation satellites. Analysis of the SAR data over time revealed that the area between S. Agostino and Mirabello villages underwent postseismic ground subsidence. Specifically, the displacement time series in the region displayed a slight initial uplift, followed by a rapid subsidence that gradually decreased over a period of approximately three months. This widespread pattern of ground displacement can be attributed to the extensive liquefaction phenomena observed a few days after the main earthquake. These phenomena, such as the emergence of sand boils and water leaks from cracks, typically result in immediate ground settlements following a seismic event. However, the delayed attainment of asymptotic settlement after approximately three months suggests a process of post-liquefaction consolidation. To test this hypothesis, we employed an analytical method to estimate the consolidation settlement caused by the dissipation of excess pore pressure induced by the earthquake. The simulated settlements align with the observed data both spatially and temporally. This provides further validation to the hypothesis that the dissipation of excess pore pressure induced by the earthquake loading played a significant role in the postseismic ground subsidence.*

1. Introduction

On the 20th of May 2012, the Emilia-Romagna region in northern Italy was struck by an M_w 5.8 earthquake (Figure 1), resulting in devastating damage and loss of life. In the days that followed, thousands of aftershocks were recorded, six of which had a magnitude greater than 5, with the most significant aftershock, measuring M_w 5.7, occurring on the 29th of May (Govoni *et al.*, 2014). The seismic activity triggered the activation of two segments of the Ferrara-Romagna thrust system, namely the Ferrara thrusts and the Mirandola thrusts (Figure

1). While the rupture propagated eastward and downdip on the Ferrara thrust system, it moved westward on the adjacent Mirandola thrust, leading to the M_w 5.7 aftershock (Govoni *et al.*, 2014).

Notably, all aftershocks with a magnitude greater than 5 were confined within 15 days of the initial event, and more than 70% of the earthquakes took place within 3 months of the primary shock. The moment tensor solutions for the stronger events displayed a reverse focal mechanism (Scognamiglio *et al.*, 2012). The tectonic dislocation associated with both the Ferrara and Mirandola thrust sheets resulted in a regional uplift of the ground (Figure 1), on the order of several centimetres (Albano *et al.*, 2017; Tizzani *et al.*, 2013).

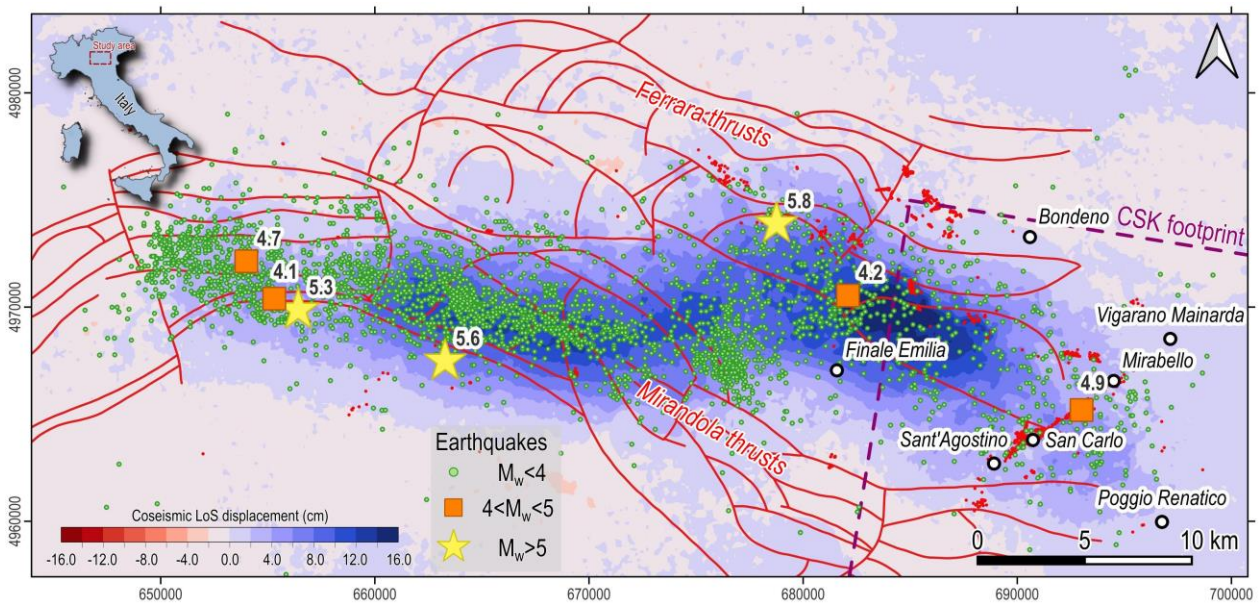

Figure 1. Sketch of the area affected by the 2012 earthquake sequence. The tectonic framework is depicted by the thrusts (red curves) of Ferrara and Mirandola. The colormap shows the unwrapped coseismic displacement field encompassing the 20 and 29 May events from the descending track of the Radarsat-2 satellite mission (modified from Tizzani et al. (2013) and Albano et al. (2017)).The red dots identify the location of liquefaction phenomena (Emergeo Working Group, 2013).

Following the main shock, various postseismic phenomena occurred. Wells in the vicinity of the epicentral area experienced a sudden increase in water level, followed by a gradual decrease that did not return to the preseismic level during the observation period (Marcaccio and Martinelli, 2012). Furthermore, periodic sampling of liquid and gaseous phases in surficial aquifers indicated the mobilization of deep-seated fluids, altering the geochemical composition of fluids and surfacing along faults and fractures (Cinti *et al.*, 2023).

Additionally, over 700 instances of liquefaction phenomena were observed, particularly in the area encompassed by the Mirabello, S. Carlo, and S. Agostino municipalities (Emergeo Working Group, 2013) (Figure 1). Sand boils, water leaks from cracks at the ground surface, and a widespread pattern of ground settlements were reported, often located along fault lines. These phenomena were accompanied by the formation of a coalescent system of flat extensional fractures with small vertical throws along preferential alignments. These fractures, sometimes spanning up to 40–50 cm, caused significant vertical offsets and the outcropping of fine sand from fractures, leading to the formation of extensive heaps.

These complex mechanisms resulted in localized subsidence (Emergeo Working Group, 2013), often causing damage to various structures, roads, walls, and vital infrastructure (Chini *et al.*, 2015). The observed phenomena can be attributed to the cyclic mobility, where failures were triggered by the upward flow of water due to excess pore pressures in deeper confined sandy soil strata. Consequently, localized ground liquefaction, flooding, sand boils, and excessive vertical settlements occurred, even after the seismic activity ceased, depending on the time needed for the dissipation of pore pressures.

Considering these events, we conducted a comprehensive study on the displacement of the Earth's surface during and after the Emilia 2012 seismic sequence, utilizing a dataset of synthetic aperture radar (SAR) images from the descending orbit of COSMO-SkyMed (CSK) constellation satellites, covering the S. Carlo, S. Agostino

and Mirabello municipalities (Figure 1). Analysis of the SAR data unveiled postseismic ground subsidence between the villages of S. Agostino and Mirabello. The observed displacement time series indicated a minor initial uplift, followed by rapid subsidence that gradually lessened over a period of approximately three months. This widespread ground displacement pattern was closely associated with the extensive liquefaction phenomena observed shortly after the main earthquake.

2. Data and methods

2.1. SAR data and processing

We analysed the displacements caused by the 20th of May 2012 earthquake, utilizing a collection of 18 synthetic aperture radar (SAR) images taken along the descending orbit of the COSMO-SkyMed (CSK) constellation satellites, at a side-looking angle of approximately 32°. This SAR dataset covers the period from the 19th of May 2012 to the 10th of May 2013, enabling us to assess both the coseismic displacement and the postseismic displacement field for a period of one year. The first postseismic data was obtained on the 23rd of May 2012, merely 3 days after the primary shock, capturing the earliest postseismic displacements. The coverage of the CSK data frames can be seen in Figure 1. A total of 55 interferograms were generated from the available SAR data and processed using the well-known small baseline subset (SBAS) algorithm (Berardino *et al.*, 2002), yielding a comprehensive spatial map showcasing the average displacement velocity within the surveyed area, as well as the displacement time series for each coherent distributed target (DT) in the scene. Details about the processing steps and the adopted parameters are reported in Albano et al., (2017). The SBAS processing returned 97,902 DT measurement points over an area of approximately 1270 km^2 (density of approximately 80 DT/km^2). InSAR measures the radar Line-of-Sight (LoS)-projected component of the surface displacements, which is a combination of both horizontal and vertical ground movements. To retrieve the vertical component, we assumed that almost all the observed LoS displacements are due to vertical ground movements only, at least in the Mirabello – S. Agostino area. Hence, we neglected the horizontal component, and we calculated the vertical displacement for each DT time-series according to Eq. (1):

$$d_v = \frac{d_{LoS}}{\cos(\theta)} \tag{1}$$

Where d_v is the vertical displacement, d_{LoS} is the displacement measured along the satellite LoS, and θ is the incidence angle of the satellite.

Finally, we spatially interpolated the displacement values of each DT using Kriging interpolation techniques (Krige, 1951). The latter include a variety of least-squares methods that provide predictions with the minimum variance of the investigated variable (Oliver and Webster, 2014; Saroli *et al.*, 2020; Spadi *et al.*, 2022).

First, a preliminary exploratory spatial analysis of DT displacements has been conducted to recognize possible correlations, trends, and outliers. Then, the experimental variogram has been estimated to identify the presence of possible anisotropies in the data. Finally, the experimental variogram has been fitted with a gaussian plus nugget model defined by Eq. (2) (Oliver and Webster, 2014):

$$f(x) = \begin{cases} c_0 + c\left\{1 - exp\left(-\frac{h^2}{a^2}\right)\right\}, & 0 < h \\ 0 \quad , & h = 0 \end{cases} \tag{2}$$

where h is the lag distance, c_0 is the nugget, c_0+c is the sill, and a is a distance parameter, proportional to the effective range (r) according to equation $r = \sqrt{3a}$. The complete analysis has been performed with the geostatistical package Gstat (Pebesma, 2004) and experimental data have been interpolated with ordinary kriging, together with the associated variance (or standard deviation).

2.2. Liquefaction analysis

We collected several geotechnical surveys from the on-line database of the Emilia Romagna region (http://geo.regione.emilia-romagna.it/geocatalogo/), carried on near the zones acknowledged as subsiding by InSAR. The collected surveys consist of boreholes, water wells, mechanical and electrical cone penetrometer test (CPT–CPTE) extended at variable depths, from just a few to more than 50 meters.

We then evaluated the susceptibility of each subsoil stratum to liquefaction by computing the safety factor (FS) expressed by the following formula (Eq.3):

$$FS = \frac{CRR}{CSR} \tag{3}$$

where CSR (cyclic stress ratio) and CRR (cyclic resistance ratio) are dimensionless factors quantifying, respectively, the seismic action and the soil resistance to liquefaction. The CSR was computed with the classical equation proposed by Seed and Idriss (1971) (Eq.4), as a function of the peak horizontal acceleration (a_{max}), the vertical effective overburden stress (σ'_{v0}), and a stress reduction factor accounting for the flexibility of the soil deformation profile (r_d). The CRR was expressed as product between a reference value ($CRR_{7.5}$) obtained for a 7.5 magnitude seismic event and a factor accounting for the moment magnitude (M_w) of the considered earthquake (Eq.5). The $CRR_{7.5}$ was related to the CPTE tip resistance using the well-known relations given by Robertson and Wride (1998).

$$CSR = 0.65 \cdot \left(\frac{a_{max}}{g}\right) \cdot \left(\frac{\sigma_{v0}}{\sigma'_{v0}}\right) \cdot r_d \tag{4}$$

$$CRR = CRR_{7.5} \cdot \left(\frac{M_w}{7.5}\right)^{-2.56} \tag{5}$$

Finally, the volumetric strains induced by liquefaction at different depths could be computed with the empirical procedure proposed by Zhang et al. (2002). In this calculation, the volumetric strains are assumed to coincide with the vertical strains, as is reasonable considering the large areal extension and the limited thickness of the liquefied soil layer.

3. Results and discussion

3.1. InSAR-derived ground displacements

The coseismic LoS displacement pattern on 23 May 2012 (Figure 2a) shows that the ground moved toward the satellite (positive values) over an area encompassing the seismic activity in the hanging wall of the main shock, close to the town of Finale Emilia. A significant component of this motion involves uplift across the Ferrara thrusts (Figure 1).

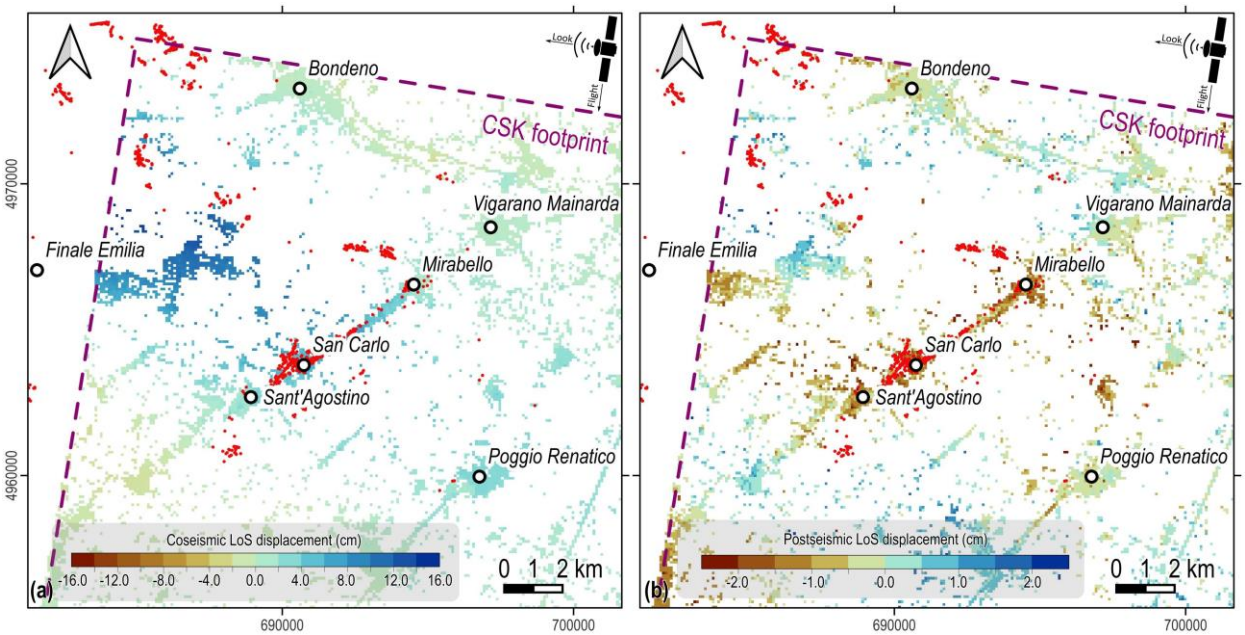

Figure 2. Ground displacement field encompassing the entire seismic sequence from the CSK SAR data. (a) Coseismic LoS displacement field associated with the 20 May event (19–23 May). (b) Cumulative postseismic LoS displacement field (23 May 2012 to 10 May 2013). The red circles indicate the location of liquefaction phenomena.

Although the obtained displacement lobe partially images the extent of the deformed area, it perfectly overlies the coseismic displacement pattern retrieved by the processing Radarsat-2 (RSAT-2) SAR images (Figure 1) (Albano *et al.*, 2017; Tizzani *et al.*, 2013).

The cumulative postseismic LoS displacements after approximately 1 year following the main shock (i.e., from 24 May 2012 to 11 May 2013) (Figure 2b) encompass the entire postseismic phase and show a complex deformation pattern. A main area of positive LoS displacements (representative of ground movements toward the sensor) with a displacement peak of approximately 3.5 cm is found to the NW, approximately overlapped to the area that experienced the maximum coseismic uplift (Figure 2a). In this area, the uplift rate is quite fast given that more than 50% of the recorded postseismic displacement occurred in the first 2 to 3 months after the earthquake. The spatial correspondence with both the aftershock epicentres and the coseismic ground displacement pattern suggests that the observed postseismic displacements have a tectonic origin, as the resulting from both analytical and numerical models (Albano *et al.*, 2017; Cheloni *et al.*, 2016).

Proceeding to the NE, the area between S. Agostino and Mirabello villages has undergone postseismic ground subsidence (negative values in Figure 2b, representing movements away from the sensor). Such diffused pattern of ground displacements overlaps with widespread liquefaction phenomena observed in the area a few days after the main shock (red circles in Figure 2b). Such phenomena (i.e., sand boils and water leaks from cracks) generally produce ground settlements not only in the affected area but also where the liquefaction phenomena are not recognized (Chini *et al.*, 2015). We converted postseismic LoS displacements in equivalent vertical movements according to Eq.1, and we produced vertical displacements maps at four postseismic epochs by means of Kriging interpolation. Such maps (Figure 3) highlight a rapid subsidence that asymptotically decreases to values up to 3 cm over approximately 3 months.

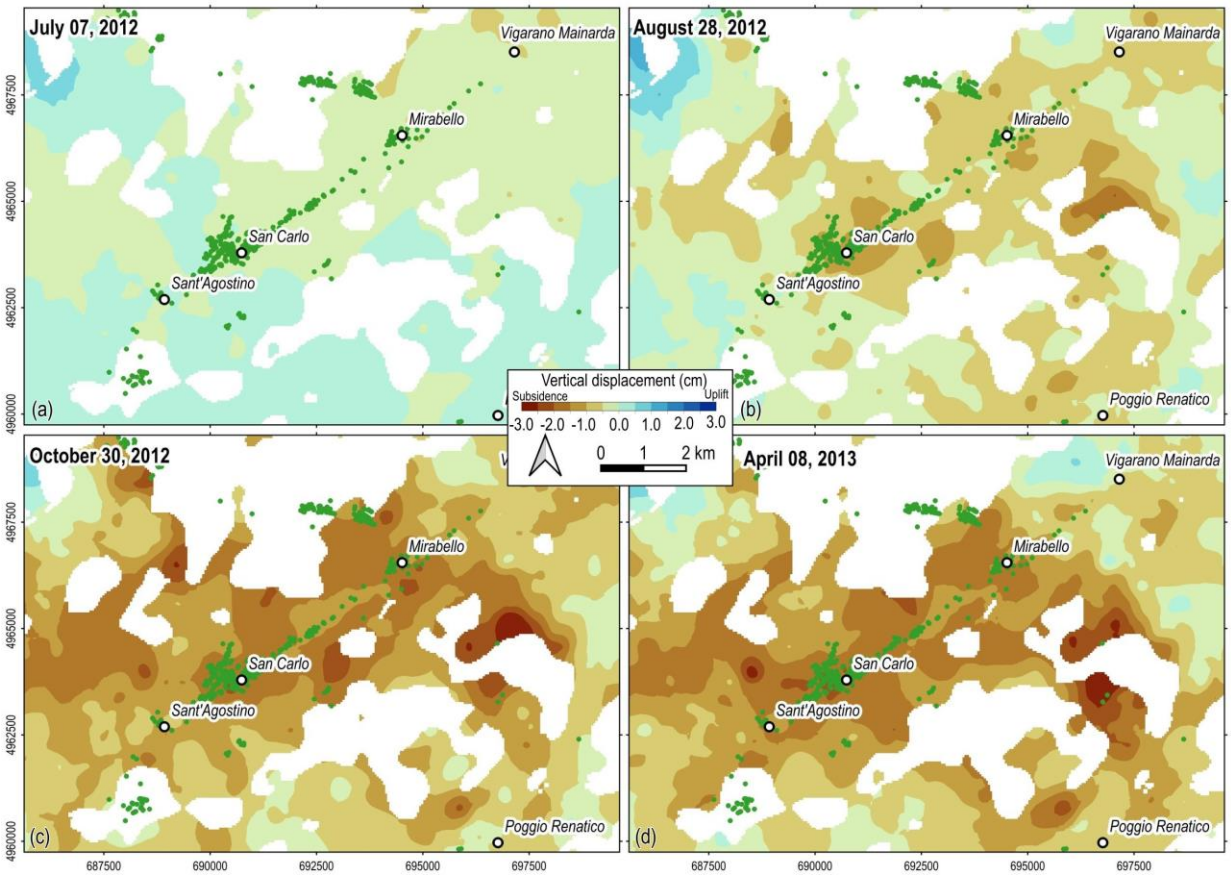

Figure 3. Cumulated vertical ground displacement maps at (a) July 07, 2012, (b) August 28, 2012, (c) October 30, 2012, and (d) April 08, 2013, computed from the Line-of-Sight InSAR ground displacement over the Mirabello, S. Carlo, and S. Agostino municipalities. Maps are banked on the areas where the prediction variance is larger than the third quantile of the variance distribution. The green dots identify the location of the observed liquefaction phenomena.

The subsidence decay is more appreciable by looking at the DT vertical time series over the S. Agostino, S. Carlo and Mirabello municipalities (Figure 4), which highlight that the whole area is affected by a transient subsidence phenomenon, dissipating almost three months after the mainshock and reaching maximum values up to -5 cm.

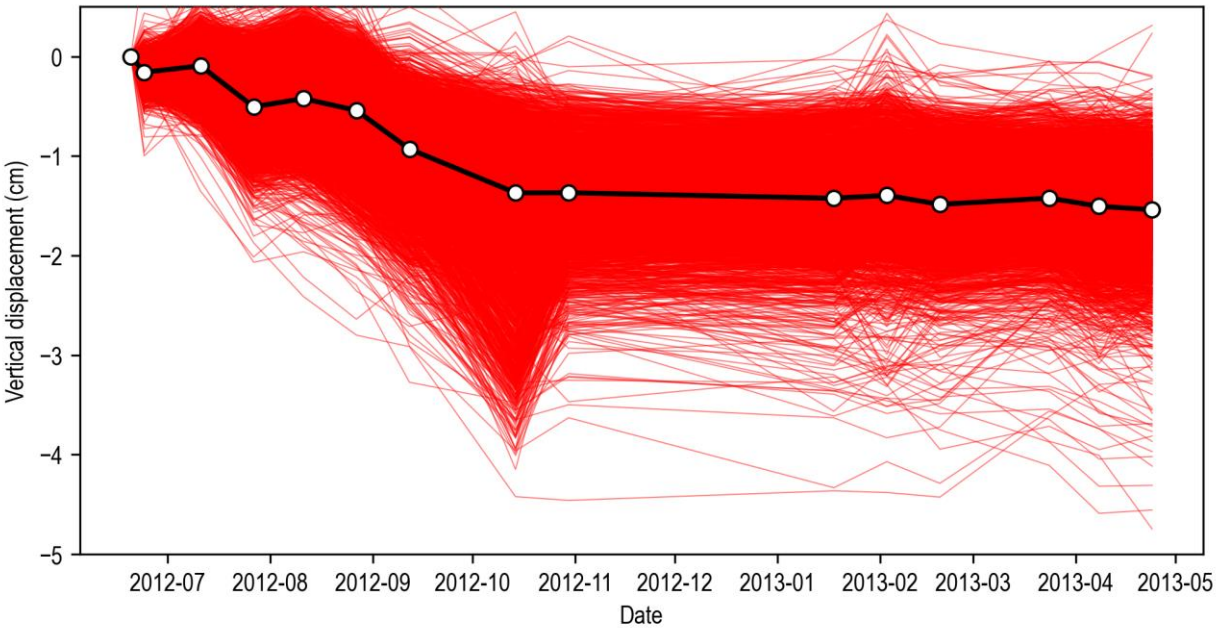

Figure 4. Postseismic vertical displacement time-series (referred to the 23 May 2023) plotted for all the DT points (approximately 3000) falling in the area between S. Agostino and Mirabello villages (Figure 3). Each red line corresponds to a single DT point. The black line identifies to the mean trend.

3.1. Liquefaction analysis results and settlement estimation

All the available geotechnical surveys repeatedly showed the presence of deposits and flood fans in the topsoil portion (up to 10–15 m form the first ground level) with strata composed of alternations of sands, sandy silts, and sandy clays. Some local presence of peat and organic soils was systematically found at deeper levels. The profiles of the classification index I_c (Robertson, 1990), computed from 13 CPTE (Figure 5b) show the presence of a fine to medium sandy layer at depths ranging between 9 and 13 m. This layer, which was found in almost all loggings, including those far more than 1 km from the investigated areas, is always submerged, being the water table recorded by piezometric measurements varying between 2 and 6 m below the ground surface.

The susceptibility of each soil layer to liquefaction was performed assuming an acceleration a_{max}= 0.22 g. Such a value was found in this area from Bozzoni et al. (2012), who performed local site response analyses. Such value is consistent with the moment magnitude of the May 20, 2012, event (M_w= 5.9). It is just slightly lower than the acceleration recorded at the Mirandola station (MRN) (a_{max}≈ 0.26 g), located at about 12 km from the epicentre (the study area is located at approximately 16 km from the epicentre). The close occurrence of two aftershocks, 4 min and 11 h, respectively after the mainshock, respectively, may have contributed to triggering the phenomenon (Sinatra and Foti, 2015).

The FS values were computed with Eq. (3) at variable depths on each of the CPTE tests, assuming a water level 3.5 m deep below ground surface. The FS profiles, cumulatively reported in (Figure 5c), together with the mean trend and standard deviation, repetitively, show that the safety factor is systematically lower than unity (i.e., the soil is susceptible to liquefaction) for the sandy layer located at depths between 8 and 13 m. By combining this result with the measured CPTE penetration resistances, the volumetric strains induced by liquefaction at different depths could be computed according to the empirical procedure proposed by Zhang et al. (2002).

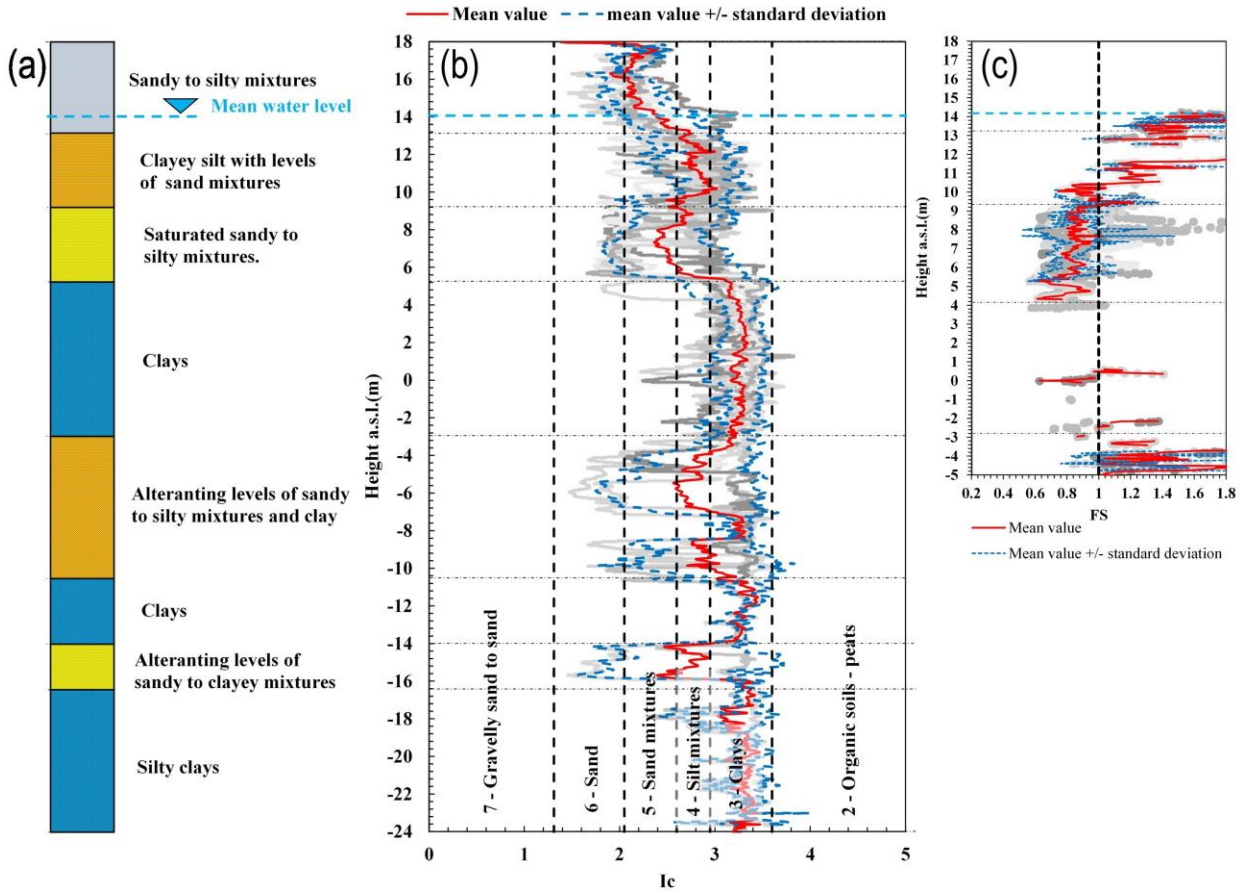

Figure 5. (a) Typical subsoil stratigraphy of the investigated area from borehole loggings. (b) I_c profile (Robertson, 1990) obtained from different electrical CPT tests with indication of mean trend (red line) +/− the standard deviation (blue lines). (c) Evaluation of liquefaction safety factor, FS, according to the Robertson and Wride (1998) method, for CPTE with indication of mean trend (red line) +/− the standard deviation (blue lines).

Finally, the settlements induced by liquefaction were estimated by integrating strains with depth. This analysis reveals a ground subsidence ranging between 6 and 10 cm. Despite the noticeable approximations of the method, there is a good repeatability of the results, which show the susceptibility to liquefaction of the sandy strata located between 9 and13 m from the ground.

Despite the computed absolute values being higher than those obtained through InSAR (refer to Figure 3 and Figure 4), there exists a qualitative consistency between the calculations and measurements, indicating a potential correlation between subsidence and subsoil characteristics. However, this quantitative comparison necessitates careful consideration. The disparity between predictions and measurements could be attributed to the presence of two distinct ground displacement phenomena in the study area: (i) tectonic postseismic deformation leading to ground uplift, and (ii) liquefaction-induced compaction resulting in ground subsidence. The intricate interplay of these phenomena, alongside the suboptimal temporal sampling provided by SAR data, renders precise estimation of ground movements challenging. Additionally, the computation of liquefaction-induced settlements relies on empirical relationships, introducing significant uncertainties into the analysis.

4. Conclusions

In conclusion, the Emilia-Romagna region in northern Italy endured significant devastation and aftershocks following the Mw 5.9 earthquake of May 20, 2012. The subsequent studies revealed a complex relationship between the ground subsidence and the underlying subsoil characteristics. The post-seismic ground subsidence, observed to gradually decrease over approximately three months, was primarily attributed to the widespread liquefaction phenomena following the main earthquake. Notably, the disparity between the

computed absolute values and the InSAR measurements highlights the intricate interplay between tectonic post-seismic deformation and liquefaction-induced compaction. Thus, while the qualitative consistency between calculations and measurements suggests a correlation, the presence of multiple ground displacement phenomena and empirical uncertainties emphasizes the need for careful consideration when interpreting these findings.

5. References

Albano, M., Barba, S., Solaro, G., Pepe, A., Bignami, C., Moro, M., Saroli, M., and Stramondo, S. (2017) Aftershocks, groundwater changes and postseismic ground displacements related to pore pressure gradients: Insights from the 2012 Emilia-Romagna earthquake: The 2012 Emilia-Romagna Earthquake. *Journal of Geophysical Research: Solid Earth* 122(7): 5622–5638.

Berardino, P., Fornaro, G., Lanari, R., and Sansosti, E. (2002) A new algorithm for surface deformation monitoring based on small baseline differential SAR interferograms. *IEEE Transactions on Geoscience and Remote Sensing* 40(11): 2375–2383.

Bozzoni, F., Lai, C. G., and Scandella, L. (2012) Preliminary results of ground-motion characteristics. *Annals of Geophysics* 55(4): 12.

Cheloni, D., Giuliani, R., D'Agostino, N., Mattone, M., Bonano, M., Fornaro, G., Lanari, R., Reale, D., and Atzori, S. (2016) New insights into fault activation and stress transfer between en echelon thrusts: The 2012 Emilia, Northern Italy, earthquake sequence. *Journal of Geophysical Research: Solid Earth* 121(6): 4742–4766.

Chini, M., Albano, M., Saroli, M., Pulvirenti, L., Moro, M., Bignami, C., Falcucci, E., Gori, S., Modoni, G., Pierdicca, N., and Stramondo, S. (2015) Coseismic liquefaction phenomenon analysis by COSMO-SkyMed: 2012 Emilia (Italy) earthquake. *International Journal of Applied Earth Observation and Geoinformation* 39: 65–78.

Cinti, D., Sciarra, A., Cantucci, B., Galli, G., Pizzino, L., Procesi, M., and Poncia, P. P. (2023) Hydrogeochemical investigation of shallow aquifers before and after the 2012 Emilia seismic sequence (northern Italy). *Applied Geochemistry* 151: 105624.

Emergeo Working Group (2013) Liquefaction phenomena associated with the Emilia earthquake sequence of May–June 2012 (Northern Italy). *Natural Hazards and Earth System Sciences* 13(4): 935–947.

Govoni, A., Marchetti, A., De Gori, P., Di Bona, M., Lucente, F. P., Improta, L., Chiarabba, C., Nardi, A., Margheriti, L., Agostinetti, N. P., Di Giovambattista, R., Latorre, D., Anselmi, M., Ciaccio, M. G., Moretti, M., Castellano, C., and Piccinini, D. (2014) The 2012 Emilia seismic sequence (Northern Italy): Imaging the thrust fault system by accurate aftershock location. *Tectonophysics* 622: 44–55.

Krige, D. G. (1951) A statistical approach to some basic mine valuation problems on the Witwatersrand. *Journal of the chemical metallurgical & mining sociaty of South Africa* 52(6).

Marcaccio, M., and Martinelli, G. (2012) Effects on the groundwater levels of the May-June 2012 Emilia seismic sequence. *Annals of Geophysics* 55(4): 38.

Oliver, M. A., and Webster, R. (2014) A tutorial guide to geostatistics: Computing and modelling variograms and kriging. *CATENA* 113: 56–69.

Pebesma, E. J. (2004) Multivariable geostatistics in S: the gstat package. *Computers & Geosciences* 30(7): 683–691.

Robertson, P. K. (1990) Soil classification using the cone penetration test. *Canadian Geotechnical Journal* 27(1): 151–158.

Robertson, P. K., and Wride, C. (Fear) (1998) Evaluating cyclic liquefaction potential using the cone penetration test. *Canadian Geotechnical Journal* 35(3): 442–459.

Saroli, M., Albano, M., Modoni, G., Moro, M., Milana, G., Spacagna, R.-L., Falcucci, E., Gori, S., and Scarascia Mugnozza, G. (2020) Insights into bedrock paleomorphology and linear dynamic soil properties of the Cassino intermontane basin (Central Italy). *Engineering Geology* 264: 105333.

Scognamiglio, L., Margheriti, L., Mele, F. M., Tinti, E., Bono, De Gori, P., Lauciani, V., Lucente, F. P., Mandiello, A. G., Marcocci, C., Mazza, S., Pintore, S., and Quintiliani, M. (2012) The 2012 Pianura Padana Emiliana seimic sequence: locations, moment tensors and magnitudes. *Annals of Geophysics* 55(4): 5.

Seed, H. B., and Idriss, I. M. (1971) Simplified Procedure for Evaluating Soil Liquefaction Potential. *Journal of the Soil Mechanics and Foundations Division* 97(9): 1249–1273.

Sinatra, L., and Foti, S. (2015) The role of aftershocks in the liquefaction phenomena caused by the Emilia 2012 seismic sequence. *Soil Dynamics and Earthquake Engineering* 75: 234–245.

Spadi, M., Tallini, M., Albano, M., Cosentino, D., Nocentini, M., and Saroli, M. (2022) New insights on bedrock morphology and local seismic amplification of the Castelnuovo village (L'Aquila Basin, Central Italy). *Engineering Geology* 297: 106506.

Tizzani, P., Castaldo, R., Solaro, G., Pepe, S., Bonano, M., Casu, F., Manunta, M., Manzo, M., Pepe, A., Samsonov, S., Lanari, R., and Sansosti, E. (2013) New insights into the 2012 Emilia (Italy) seismic sequence through advanced numerical modeling of ground deformation InSAR measurements. *Geophysical Research Letters* 40(10): 1971–1977.

Zhang, G., Robertson, P. K., and Brachman, R. W. I. (2002) Estimating liquefaction-induced ground settlements from CPT for level ground. *Canadian Geotechnical Journal* 39(5): 1168–1180.